

Numerical Investigation of Geometric Effects on Infrared Characteristics of Multi-stream Serpentine Nozzles

Yuxing Wu[1], Li Zhou[1], Jie Shi[1], Yubo Meng[1] & Zhanxue Wang[1]

[1]School of Power and Energy, Northwestern Polytechnical University, Xi'an 710072, China

Abstract

The multi-stream serpentine nozzle is a critical configuration for balancing the multi-stream matching of adaptive cycle engines with the stringent infrared (IR) stealth requirements of advanced fighters. To elucidate the influence mechanisms of key geometric parameters on its IR radiation characteristics, this paper conducts a parametric sensitivity study on the shield ratio (SR) and aspect ratio (AR) using numerical simulation methods. The results indicate that under the baseline configuration, the high-temperature core gas is fully enveloped by the bypass cold stream, rendering the overall IR signature dominated by gas radiation. Meanwhile, due to the coupling effect of the high-curvature duct and the flat exit, radiation levels in the vertical detection plane are significantly higher than those in the horizontal plane, exhibiting strong spatial asymmetry. As the SR increases, the shielding effect on internal high-temperature walls is enhanced; when the SR exceeds 0.55, complete occlusion is achieved, leading to a drop of over 90% in wall radiation and compelling a transition of the dominant radiation source from the wall to the gas. Concurrently, increasing the aspect ratio flattens the nozzle exit, significantly enhancing the mixing between the jet plume and the atmosphere, effectively truncating the high-temperature core region, and driving a monotonic decrease in the dominant gas radiation by up to 30%.

Keywords: Multi-stream serpentine nozzle; Adaptive engine; Infrared radiation; Numerical simulation

1. Introduction

The Adaptive Cycle Engine (ACE), owing to its unique variable thermodynamic cycle characteristics [1-2], has become a crucial development direction for next-generation advanced fighter propulsion. However, it also imposes more stringent multi-stream matching challenges on the exhaust system. Meanwhile, modern warfare scenarios demand highly rigorous infrared stealth capabilities for fighter jets, making the low-observable design of the exhaust system indispensable [3]. By utilizing a highly curved duct design, the serpentine nozzle can effectively shield the high-temperature components inside the engine, exhibiting excellent infrared suppression capabilities. Consequently, it has been widely regarded as the core configuration for the stealth exhaust systems of advanced fighters [4]. To balance the complex multi-stream matching with rigorous infrared stealth requirements, the integration of multi-stream and serpentine configurations has become an inevitable trend.

Extensive research has been conducted on the infrared radiation characteristics of conventional exhaust systems, including axisymmetric, two-dimensional, single-stream serpentine, and three-bearing swivel vectoring nozzles [5-7]. As exhaust systems evolve, applying a serpentine configuration to multi-stream designs introduces strong coupling between complex geometry and multi-stream flows. This significantly complicates both the flow field and infrared performance. Currently, investigations into multi-stream serpentine nozzles primarily focus on their complex internal flow physics and aeroacoustic characteristics [8-10]. Existing literature indicates [11] that geometric design parameters, such as the throat AR and SR, substantially affect the mixing efficiency of the multiple streams. For instance, the serpentine configuration induces a strongly non-uniform mainstream and streamwise vortices, generating complex shock-wave structures in the mixing section, which inevitably leads to aerodynamic losses. The complex mixing of multiple streams not only causes aerodynamic losses but also significantly alters the temperature field distribution inside the nozzle, making the evaluation of the infrared stealth performance of multi-stream serpentine nozzles a gradual focus of academic attention. Xu et al. [12] pointed out that under various operating conditions, the gas radiation from the nozzle

interior and the exhaust plume, along with the wall hot-spot effects induced by geometric curvature, play a dominant role in the overall infrared signature. Nevertheless, due to the complex occlusion and mixing characteristics within the multi-stream serpentine nozzle, its infrared radiation signature is highly sensitive to geometric parameter variations. Therefore, conducting a parametric study on the infrared radiation characteristics of multi-stream serpentine nozzles to ascertain the influence laws of key geometric parameters is of great significance for their further infrared optimization design.

To this end, this paper investigates the parametric sensitivity of geometric parameters and their influence on the IR signature of multi-stream serpentine nozzles. Based on numerical simulations, this study performs a comparative analysis of multi-stream serpentine nozzles with different shield ratios (SR) and aspect ratios (AR). By quantifying the correlations between each key geometric parameter and the infrared radiation intensity, this research aims to elucidate the influence mechanisms of key geometric parameters on the infrared radiation characteristics of multi-stream serpentine nozzles. Ultimately, it provides a theoretical foundation and data reference for the comprehensive infrared stealth optimization design of multi-stream serpentine exhaust systems for next-generation advanced fighters.

2. Geometric model

The multi-stream serpentine nozzle consists of a straight section, a mainstream convergent section, a mainstream divergent section, tertiary stream passages, and a mixing section, as illustrated in Fig. 1. Both the mainstream convergent and divergent sections are defined by an S-shaped centerline based on the Lee curve [13] and a series of cross-sections distributed along this trajectory. The mainstream convergent section features a round-to-rectangular transition structure, with a rectangular throat cross-section. Both the mainstream divergent section and the mixing section have rectangular cross-sections, maintaining a consistent width with the throat. The upper and lower tertiary stream passages are both designed as rectangular convergent ducts. The nozzle employs simplified parallel and uniform inlets for the core and bypass streams, excluding components such as mixers and tail cones. Within the straight section of the nozzle, the core inlet diameter is 521 mm, and the bypass inlet diameter is 550 mm. Additionally, the tertiary stream inlet area is 0.05 m², and the throat area is 0.16 m².

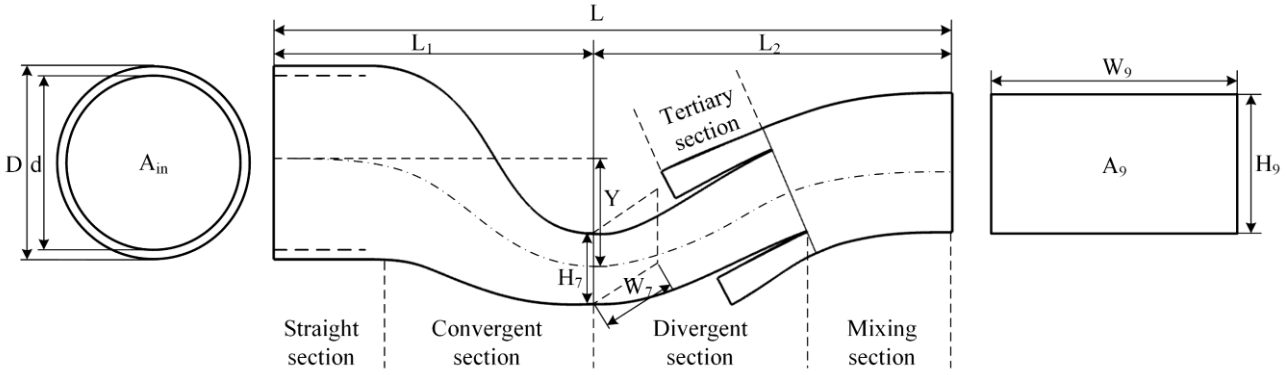


Figure 1 – Geometric model of multi-stream serpentine nozzle

In this study, key dimensionless design parameters—namely the length-to-diameter ratio (LDR = L/D), shield ratio (SR = Y/D), and aspect ratio (AR = W_7/H_7)—are selected to investigate the influence of geometric design parameters on the infrared radiation characteristics of the multi-stream serpentine nozzle. The geometric parameters of the adopted baseline model are summarized in the table below.

Table 1 – Baseline multi-stream serpentine nozzle design parameters

Parameters	LDR	SR	AR
Value	3	0.55	4

3. Numerical simulation methods

3.1 CFD simulation method

Ansys Fluent is employed to compute the aerodynamic characteristics, accurately capturing the highly non-uniform distributions of temperature, pressure, and species concentrations across the flow fields to ensure the fidelity of subsequent infrared simulations. The three-dimensional compressible Reynolds-Averaged Navier-Stokes (RANS) equations are solved using the finite volume method with a second-order upwind spatial discretization scheme, coupled with the Shear Stress Transport (SST) $k-\omega$ two-equation turbulence model.

The Discrete Ordinates (DO) model is selected to calculate the radiative heat transfer within the nozzle, accounting for the absorption and emission characteristics of the participating gas media. Furthermore, the species transport model is activated to determine the spatial distributions of the combustion products throughout the internal and external flow fields. The working fluid is modeled as an ideal gas, and the variation in its dynamic viscosity is determined by Sutherland's law.

Based on the geometric symmetry of the multi-stream serpentine nozzle, a symmetric meshing strategy is adopted. As illustrated in Fig. 2, the computational domain encompasses both the nozzle and the far-field regions, which are spatially discretized by hexahedral grids. The primary flows enter the nozzle via the core, bypass, and third-stream inlets, respectively, and are subsequently discharged into the far field after internal multi-stream mixing to undergo secondary mixing with the ambient atmosphere. By encompassing the internal core flow regions, the multi-stream confluence zone, and the jet expansion shear layer, the computational domain accurately captures the essential flow features.

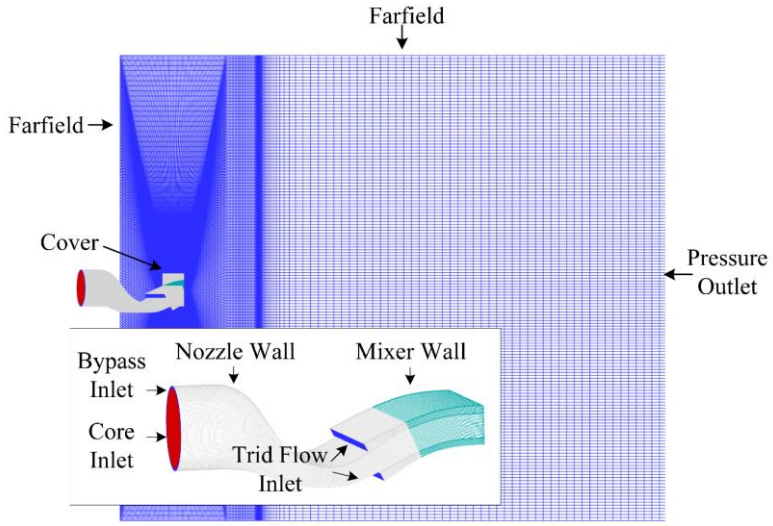


Figure 2 – Computational domain grid

The inlet boundary conditions for the core, bypass, and tertiary streams of the multi-stream nozzle are all specified as pressure inlets. Based on the design operating conditions of the variable cycle engine exhaust system, the total temperature T^* and total pressure p^* are prescribed, with the nozzle pressure ratio (NPR) of the core stream set to 5 and that of the tertiary stream set to 1.89. No-slip boundary conditions are applied to all solid walls of the nozzle and the mixing section. The far-field boundary is configured according to the atmospheric parameters at ground-level operating conditions, specifying a uniform freestream Mach number Ma_∞ and total temperature T^*. The species concentrations of the combustion products at the core inlet are determined based on the complete combustion assumption, whereas the gas species concentrations at the bypass, tertiary, and far-field inlets are specified as standard air. The detailed flow field boundary parameters are summarized in Table 2, where the species concentrations are expressed in terms of mole fractions.

Table 2 – Flow field boundary conditions

Boundary Conditions	T^*/K	p^*/KPa	Ma_∞	f_{CO_2}	f_{H_2O}	f_{O_2}
Core inlet	1247	506.526	\	0.13	0.13	0
Bypass inlet	507	575.931	\	0	0	0.21
Tertiary inlet	300	191.808	\	0	0	0.21
Farfield inlet	300	101.325	0.05	0	0	0.21

3.2 Infrared radiation simulation method

To accurately characterize the spectral absorption and emission properties of typical infrared-active components, such as H_2O, CO_2, and CO, in the internal and external flow fields of the multi-stream serpentine nozzle, the Statistical Narrow-Band (SNB) model [14] is employed. This model is based on the Mayer and Goody method combined with the Malkmus inverse-exponential line-strength distribution function, alongside the Curtis-Godson approximation to handle the inhomogeneous gas paths along the line of sight. When using the Malkmus narrow-band model, the spectral transmittance of a gas element is calculated as follows:

$$\tau_\lambda = \exp\left[-\frac{2\bar{\gamma}}{\bar{\delta}}\left(\sqrt{1+\frac{fpl\bar{\kappa}\bar{\delta}}{\bar{\gamma}}}-1\right)\right] \tag{1}$$

where the parameters $\bar{\kappa}$, $\bar{\gamma}$, and $\bar{\delta}$ denote the mean line intensity, the mean Lorentz half-width, and the mean line spacing within the narrow-band interval, respectively. These high-resolution narrow-band parameters are acquired by integrating line-by-line calculations from the CDSD-4000 [15] and HITEMP [16] high-temperature gas molecular spectroscopic databases. Furthermore, f is the species mole fraction, p is the local gas pressure, and l represents the path length of the ray element.

Addressing the severe geometric occlusion and multiple reflection effects within the multi-stream serpentine nozzle, the Discrete Transfer Method (DTM), identical to that in Ref. [17], is utilized to compute the infrared radiation characteristics. The principle of the DTM is illustrated in Fig. 3. This method treats the solid wall elements as absorption and emission sources of infrared radiation. By solving the radiative transfer equations between the boundaries of each element, the effective irradiation of the solid walls is calculated, and the effective radiance is subsequently obtained based on the diffuse reflection assumption. On this basis, the radiative transfer equation along the characteristic rays emitted from the detector is solved. The total infrared radiation intensity I of the target relative to the detector is acquired by integrating the gas radiance and the wall effective radiance over the pixel plane.

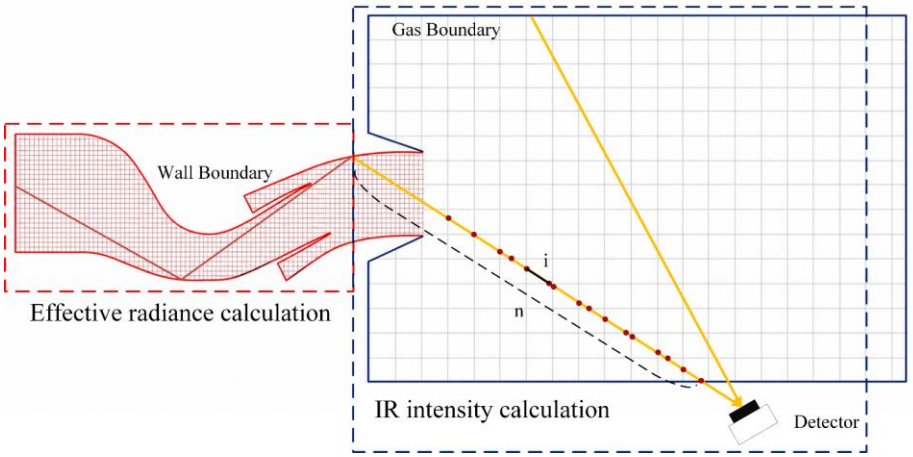


Figure 3 – Discrete transfer method schematic diagram

Specifically, the core governing equations for the aforementioned physical processes are described as follows. First, under the diffuse gray body assumption and accounting for the multiple reflection effects inside the nozzle, the discrete equation for the effective spectral radiance $L_{\lambda,\mathrm{w}}$ of a wall element is formulated as:

$$L_{\lambda,\mathrm{w}} = \varepsilon_\lambda L_{\mathrm{b}\lambda}(T_\mathrm{w}) + \frac{1-\varepsilon_\lambda}{\pi}\sum_{k=1}^{N} L_{\lambda,\mathrm{in},k}\cos\theta_k \Delta\Omega_k \tag{2}$$

where ε_λ denotes the wall emissivity; $L_{\mathrm{b}\lambda}(T_\mathrm{w})$ is the blackbody spectral radiance at the wall temperature T_w; $L_{\lambda,\mathrm{in},k}$ represents the incident spectral radiance from the k-th spatial discrete ray cast onto the wall element; θ_k and $\Delta\Omega_k$ are the ray incidence angle and the represented solid angle, respectively; and N is the total number of discrete rays over the hemispherical space.

After determining the radiance at the wall boundaries, the spatial radiative transfer process through the participating media is computed by inversely tracing the characteristic rays. The spectral radiance L_λ along the characteristic ray is accumulated as it passes through each fluid grid element, governed by the discrete transfer equation:

$$L_\lambda = J_\lambda \prod_{i=1}^{n}\tau_\lambda(i) + \sum_{i=1}^{n}\varepsilon_\lambda(i) L_{\mathrm{bi}}(i)\prod_{j=i+1}^{n}\tau_\lambda(j) \tag{3}$$

where J_λ represents the initial spectral radiance at the starting boundary of the characteristic ray in the flow field. When the ray is inversely traced and intersects the solid wall of the nozzle, this initial value strictly equals the effective spectral radiance of the wall element calculated from Eq. (2) (i.e., $J_\lambda = L_{\lambda,\mathrm{w}}$); if the ray exits the fluid domain without striking any solid geometry, J_λ assumes the background radiance. Furthermore, $\tau_\lambda(i)$ and $\varepsilon_\lambda(i)$ denote the spectral transmittance and emissivity of the i-th gas element, respectively, and $L_{\mathrm{bi}}(i)$ is the local blackbody spectral radiance of the gas element at its local temperature.

During the numerical simulation of the infrared radiation characteristics for the multi-stream serpentine nozzle, the upstream region of the core inlet is a low-pressure turbine, which is thus simplified as a gray body wall. The wall emissivity of all components is uniformly set to 0.9. The infrared calculation wavelength ranges from 3 to 5μm, and the detection distance is set to 1000m. The atmospheric absorption characteristics are calculated

using the Modtran software. The detection point arrangement scheme is depicted in Fig. 4, where a detection point is positioned at 5° intervals on both the horizontal and vertical detection planes, with the detection angle α varying from -90° to 90°.

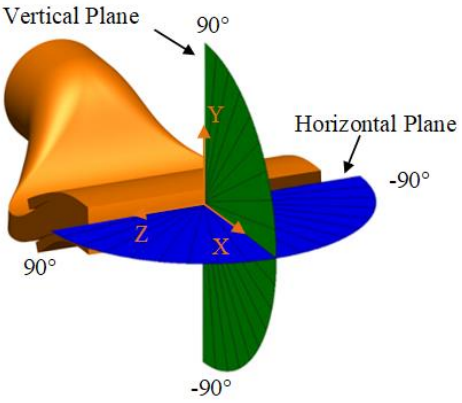


Figure 4 – Detection point layout

To evaluate the influence of grid resolution on simulation results, a mesh convergence study was conducted for the multi-stream serpentine nozzle. Three sets of grids with 4.38, 8.65, and 17.25 million cells were employed, maintaining a consistent refinement ratio in all spatial directions. The same mesh was utilized for both the aerodynamic and infrared radiation calculations. The infrared radiation intensity in the positive detection angle range of the horizontal detection plane was selected as the key variable for comparison (Fig. 5). The average relative errors for the 4.38-million and 8.65-million grids, relative to the 17.25-million fine grid, are 0.85% and 0.27%, respectively. Notably, the 4.38-million grid exhibits a larger discrepancy at large detection angles, showing a relative error of 1.77% at 85°, whereas the 8.65-million grid maintains a minimal error of only 0.07%. These results indicate that the infrared radiation characteristics achieve numerical convergence at a grid count of 8.65 million. Consequently, the 8.65-million-cell grid was adopted for subsequent simulations.

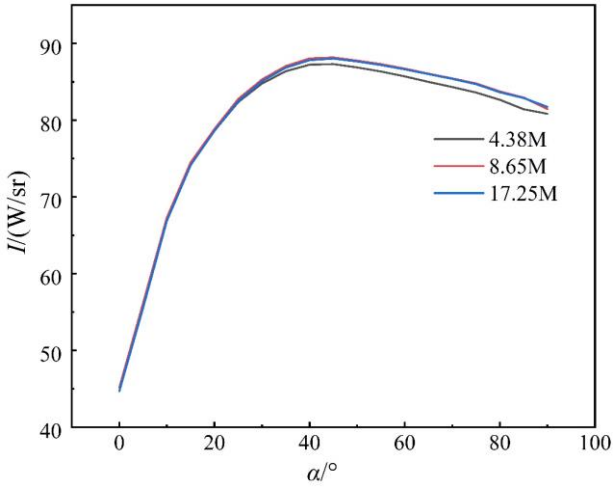


Figure 5 – Mesh convergence verification

4. Results

4.1 Baseline

The spatial distribution characteristics of the normalized infrared radiation intensity for the baseline multi-stream serpentine nozzle in the horizontal and vertical detection planes are shown in Fig. 6. In the figure, α represents the detection angle, I represents the IR radiation intensity, and I_{max} is the maximum total radiation intensity of the baseline multi-stream serpentine nozzle. For further analysis, the spatial distributions of the gas radiation, wall radiation, and total radiation intensity are presented separately in the figure. Due to the physical occlusion provided by the curved configuration, gas radiation contributes significantly more to the overall IR signature than wall radiation. Consequently, the spatial distribution of the IR intensity is primarily gas-dominated.

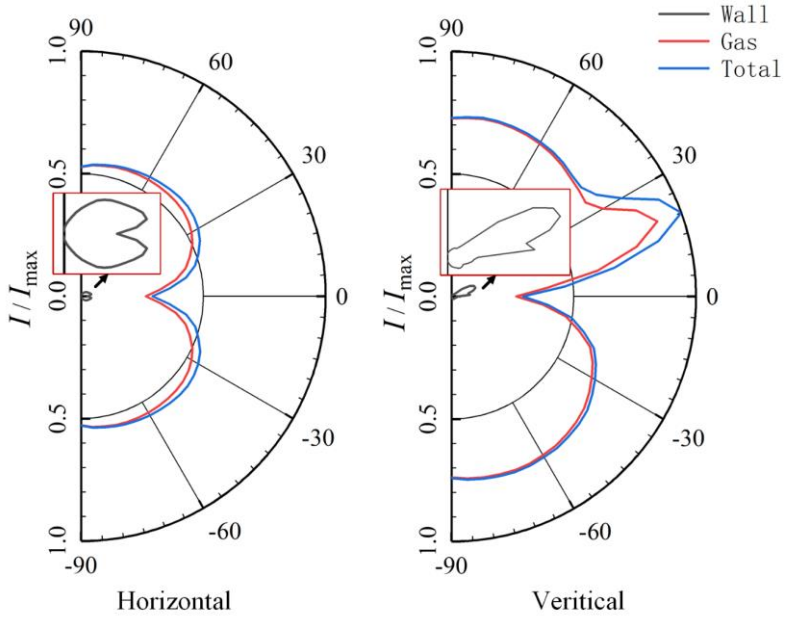


Figure 6 – Spatial distribution of normalized IR radiation intensity for the baseline nozzle

Due to the geometric symmetry of the multi-stream serpentine nozzle in the horizontal detection plane, the infrared (IR) radiation intensity distributions at positive and negative detection angles in this plane also exhibit completely symmetric characteristics. As $|\alpha|$ increases, both the gas and wall radiation intensities generally exhibit a trend of initially increasing and subsequently decreasing. Under different $|\alpha|$, the gas radiation intensity in the horizontal detection plane is significantly higher than that of the wall radiation. The peak of the total radiation intensity occurs at $|\alpha| = 45^{\circ}$.

Compared to the horizontal detection plane, the radiation from different sources in the vertical detection plane exhibits pronounced asymmetric characteristics. The overall radiation intensity is lower when $\alpha < 0$, indicating that this configuration demonstrates superior IR stealth performance against downward detection. Simultaneously, the overall contributions of wall and gas radiation in the vertical detection plane are higher than those in the horizontal plane. As $|\alpha|$ increases, the wall and gas radiation intensities in the vertical detection plane also present a general trend of initially increasing and then decreasing. Notably, both the gas and wall radiation exhibit a high-radiation zone near $\alpha = 20^{\circ}$ in the positive detection angle region of the vertical plane, which coincides with the detection angle corresponding to the total radiation peak. Furthermore, the contribution of wall radiation to the total radiation in the vertical detection plane is almost exclusively concentrated within this high-radiation zone.

According to the Stefan-Boltzmann law, the wall or gas temperature plays a decisive role in the IR radiation characteristics. Fig. 7 and 8 present the temperature distribution contours on the symmetry plane and the inner wall of the baseline multi-stream serpentine nozzle, respectively. As shown in Fig.

7, under the assumptions of uniform inflow and the absence of a real mixer, the mixing efficiency between the core and bypass streams is relatively low. The low-temperature bypass stream completely envelops the high-temperature core gas. This confinement prevents direct convective heat transfer to the walls, effectively suppressing the formation of hot-spots. Furthermore, benefiting from the complete line-of-sight (LOS) occlusion of the core inlet provided by the baseline multi-stream serpentine nozzle configuration, the core inlet remains entirely invisible across the full range of detection angles. At this time, the detectable wall temperature is maintained at a low level of approximately 300 K, ensuring that the overall IR signature of the nozzle is absolutely dominated by gas radiation.

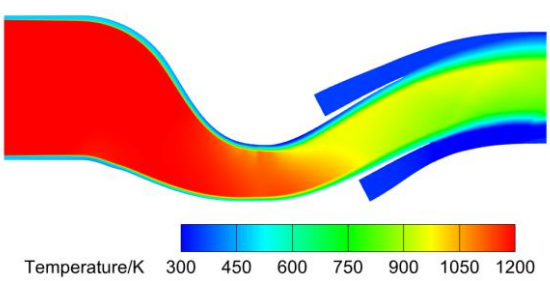


Figure 7 – Temperature distribution on the symmetry plane of the baseline model

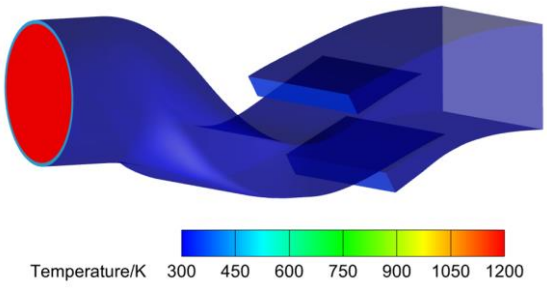


Figure 8 –Wall temperature distribution of the baseline model

Given the dominant role of gas radiation in the overall infrared radiation characteristics, this paper further

analyzes its spatial distribution laws. Gas radiation can be decoupled into two parts: the exhaust plume radiation and the gas radiation within the internal cavity of the nozzle. Figure 9 shows the 800 K temperature iso-surface of the baseline model plume. It can be seen that, constrained by the rectangular exit, the exhaust plume also exhibits pronounced two-dimensional diffusion characteristics. Under the baseline geometry of $AR = 4$, the overall spanwise width of the plume is significantly greater than its normal height. This cross-sectional shape results in a larger projected area of the high-temperature core region of the plume in the vertical detection plane, which in turn causes the overall gas radiation intensity in the vertical detection plane to be significantly higher than that in the horizontal detection plane.

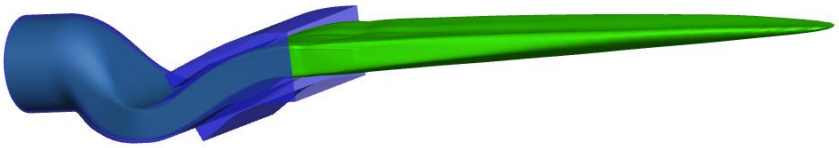


Figure 9 – 800 K temperature iso-surface of the baseline model

To elucidate the evolution mechanism of gas radiation at different detection angles, Fig. 10 presents the variation of the visible length of the plume core region with the detection angle in the horizontal detection plane. As shown in the figure, when the absolute value of the detection angle $|\alpha|$ is small, the projected area of the high-temperature core region of the plume is limited, and the gas radiation primarily originates from the high-temperature gas inside the nozzle. With the gradual increase of $|\alpha|$, the high-temperature gas inside the nozzle is gradually shielded by the wall. However, the projected area of the high-temperature core region of the exhaust plume expands rapidly, causing the plume radiation to increase rapidly and dominate the total gas radiation. Consequently, the reduced visibility of internal high-temperature gas, coupled with the expanding visible area of the external plume core, drives the initial rise and subsequent decline in gas radiation.

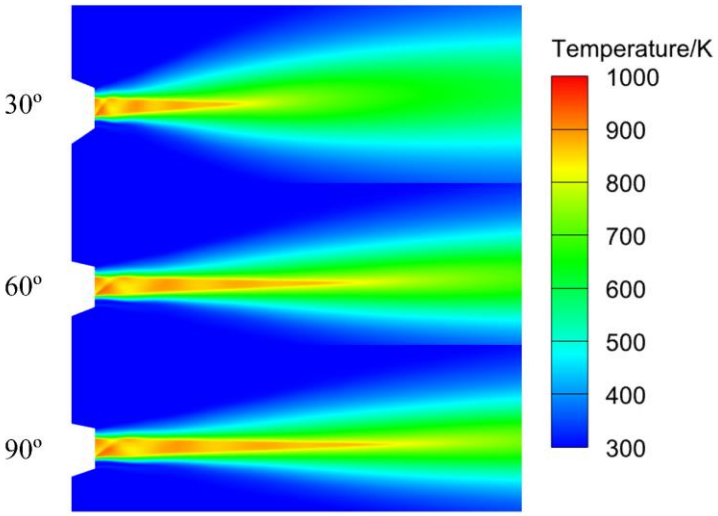


Figure 10 – Plume core length at different detection angles in the horizontal plane

In the vertical detection plane, the infrared radiation intensities of the gas and wall in the positive detection angle region experience a surge near $\alpha = 20^{\circ}$, forming a high-radiation zone with a span of approximately 10°, whose peak significantly exceeds the radiation level in the negative detection angle region. To investigate the generation mechanism of this high-radiation zone, Fig. 11 presents a schematic of the detectable region inside the nozzle. As shown, when the detection angle is 20°, the line of sight (LOS) of the detector can penetrate to the greatest extent and observe the high-temperature gas core inside the nozzle. Compared to the external exhaust plume, the gas inside the nozzle possesses higher temperature and pressure, thereby exhibiting a stronger radiation contribution capability. The sudden increase in the visible range of the internal high-temperature gas directly contributes to the emergence of the gas radiation peak at $\alpha = 20^{\circ}$. Conversely, at $\alpha = -20^{\circ}$, the visible region of the internal high-temperature gas is significantly compressed, and the detector's field of view is predominantly occupied by the low-temperature gas in the mixing section.

Simultaneously, as shown in Fig. 11, when the detection angle is 20°, the characteristic rays only need to undergo a single wall reflection to effectively receive the radiation contribution from the high-temperature wall source at the core inlet. Conversely, at -20°, rays undergo multiple reflection attenuations within the curved duct. This traps the radiation energy from upstream hot components, significantly suppressing the intensity at negative detection angles. Figure 12 illustrates the spatial distribution of the dimensionless reflected radiation intensity $I_{ref} / I_{ref,max}$, normalized by its maximum value, and the ratio of reflected radiation to total radiation η with respect to the detection angle. It can be seen that near a detection angle of 20°, the dimensionless

reflected radiation intensity I_{ref} / $I_{ref,max}$ increases rapidly and is significantly higher than that in the negative detection angle region. Nevertheless, with the expansion of the visible region of the internal high-temperature gas, both the gas radiation and the reflected wall radiation intensities exhibit a synchronous increasing trend. Consequently, the reflected radiation ratio η in this specific region does not experience a massive leap but remains relatively stable. In summary, the increase in the directly visible area of the gas at positive detection angles and the gain from single-reflection wall radiation are the two major factors leading to the generation of the high-radiation zone.

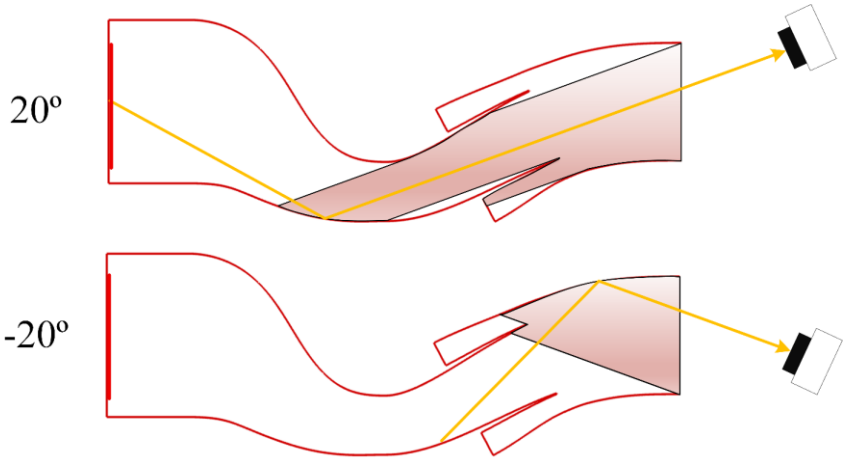


Figure 11 – Schematic of the detectable region in the vertical plane

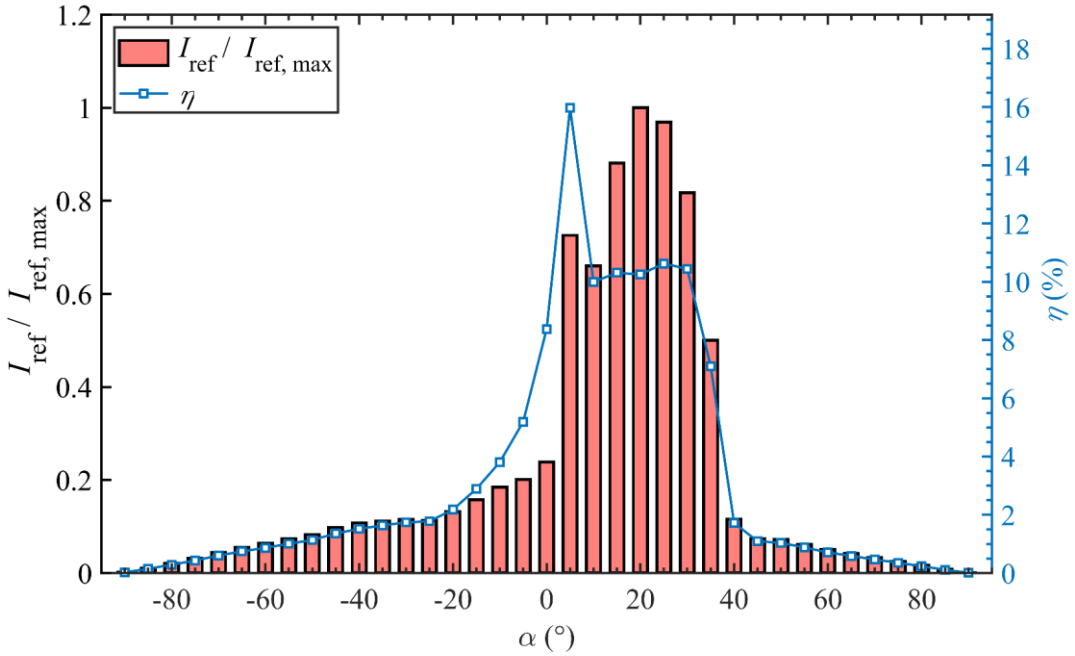
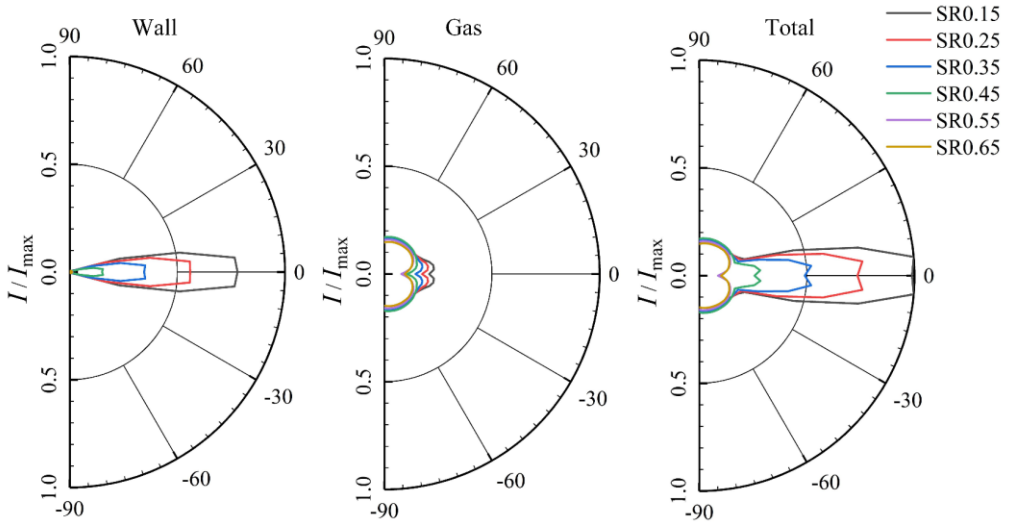


Figure 12 – Reflected radiation intensity and its ratio in the vertical plane

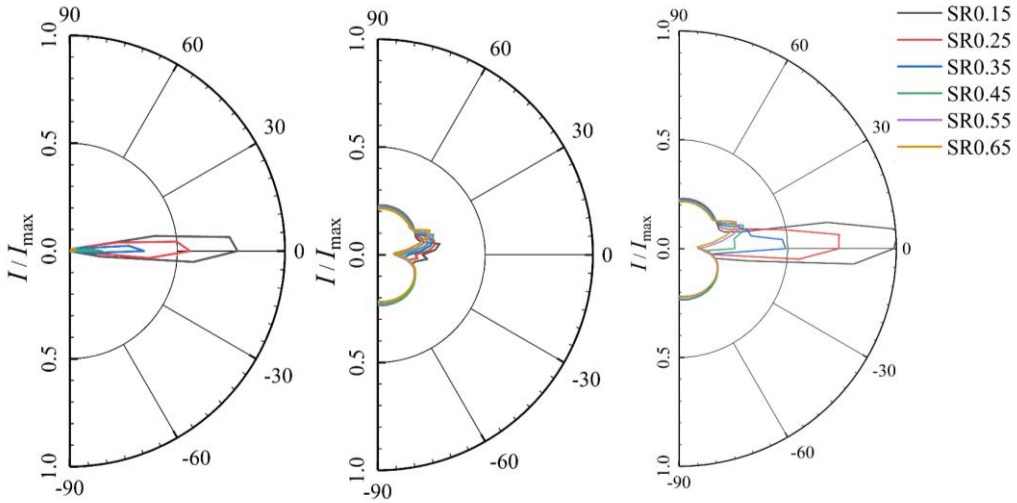
4.2 Shield Ratio

The shield ratio (SR) is a key geometric parameter affecting the shielding characteristics of the multi-stream serpentine nozzle. As the shield ratio decreases, the longitudinal offset of the multi-stream serpentine nozzle reduces, and the visible area of the upstream hot components of the nozzle increases accordingly. Based on the baseline multi-stream serpentine nozzle, this paper establishes multi-stream serpentine nozzle models with SRs of 0.15, 0.25, 0.35, 0.45, and 0.65 by solely changing the shield ratio, and obtains the spatial distributions of the infrared radiation intensity of the nozzle under different shield ratios, as shown in Fig. 13. Analysis indicates that when the shield ratio is small, the infrared radiation characteristics of the multi-stream serpentine nozzle degrade and approach those of a conventional multi-stream two-dimensional nozzle; at this point, the total infrared radiation is almost entirely dominated by the internal high-temperature wall radiation. With the gradual increase in the shield ratio, the physical shielding effect on the internal cavity is enhanced, and both the extent and intensity of the high-radiation zones of the gas and wall exhibit a significant shrinking trend. Additionally, the angular bounds of the high-radiation zones remain consistent across different SRs. The broader high-radiation zone in the horizontal plane directly elevates its overall wall radiation level above that of the vertical plane. In summary, as the shield ratio increases, the infrared radiation characteristics of the

multi-stream serpentine nozzle gradually evolve from being wall-radiation-dominated to gas-radiation-dominated.



(a) Horizontal plane



(b) Vertical plane

Figure 13 – Spatial distribution of IR radiation intensity for multi-stream serpentine nozzles with different SRs

To intuitively reveal the physical processes behind the aforementioned evolution of radiation characteristics, Figure 14 presents the infrared imaging characteristics of the wall and gas for configurations with different shield ratios from a direct rear-view perspective. At SR=0.15, the small longitudinal offset exposes a large area of the core inlet wall and the internal gas core to direct rear observation. Increasing SR to 0.45 elevates the lower duct wall, partially blocking the line of sight (LOS) and significantly compressing these visible high-temperature regions. When the SR further increases to 0.65, the high-temperature hot components at the core inlet are completely physically occluded, and obvious high-brightness regions no longer appear in the infrared imaging of the wall.

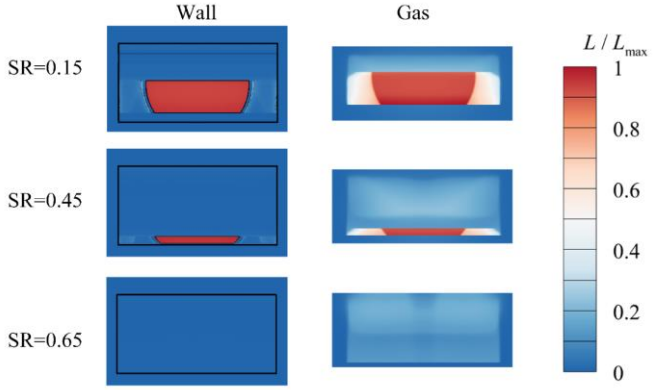


Figure 14 – Dimensionless IR radiance contours of the wall and gas for multi-stream serpentine nozzles with different SRs

The reduction in the aforementioned geometric visible area is the core driving force leading to the decrease in radiation intensity. Figure 15 quantitatively presents the variation curves of the dimensionless visible area of the core inlet, $A_{core} / A_{core,max}$, and the dimensionless radiation intensity, $I_{core} / I_{core,max}$, with respect to the shield ratio. As shown in the figure, both exhibit a highly consistent attenuation trend as the SR increases, demonstrating that the reduction in the visible area caused by the geometric offset is the core factor weakening the infrared radiation intensity of the multi-stream serpentine nozzle. Specifically, when the SR reaches 0.55, the high-temperature visible area of the core inlet is completely reduced to zero, and its direct radiation contribution to the external detection planes is also completely eliminated, which explains the phenomenon observed in Fig. 7 where the infrared radiation characteristics exhibit a significant attenuation after $SR \geq 0.55$.

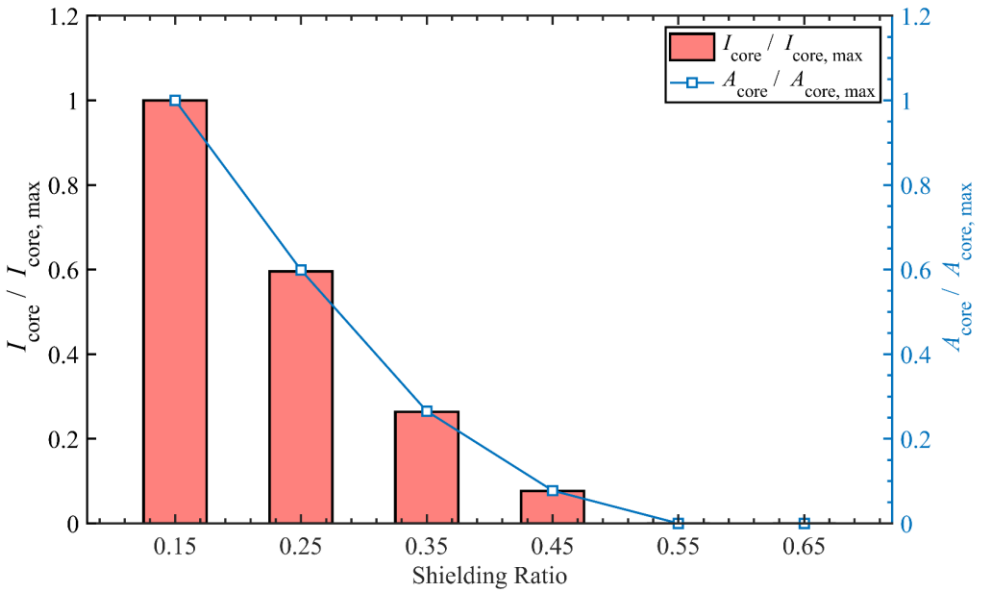
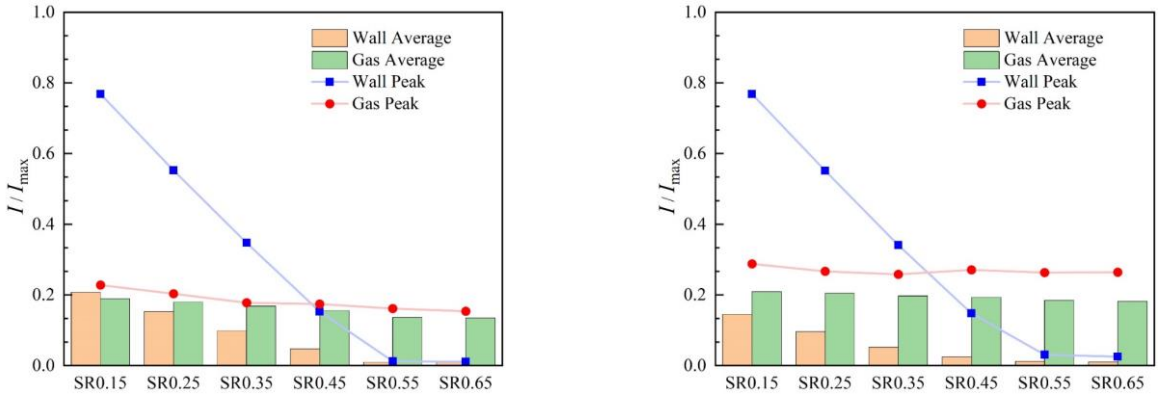


Figure 15 – Visible area and radiation intensity of the core inlet in the horizontal plane

Based on the quantitative analysis of the shielding mechanism mentioned above, Fig. 16 further calculates the global evolution laws of the average and peak radiation intensities in different detection planes. Directly affected by the progressive and eventual complete occlusion of the core inlet, the peak wall radiation in both the horizontal and vertical detection planes exhibits a precipitous downward trend with the increase of SR, with a maximum reduction exceeding 90%. In contrast, the external exhaust plume remains largely unaffected by the internal geometric occlusion. As a result, the attenuation of the peak and average gas radiation with increasing SR is significantly more gradual.

Furthermore, the phenomenon of alternating dominance between the average and peak radiation values in the figure is noteworthy. In the low shield ratio range (SR = 0.15), the wall radiation characteristics are significantly higher than the gas radiation characteristics; however, when the SR exceeds 0.45, the wall radiation is suppressed to an extremely low level, and both the average and peak values of gas radiation successfully surpass the wall radiation. This evolutionary characteristic further corroborates that, as the shield ratio increases, the overall infrared radiation signature of the multi-stream serpentine nozzle transitions from being wall-radiation-dominated to gas-radiation-dominated.



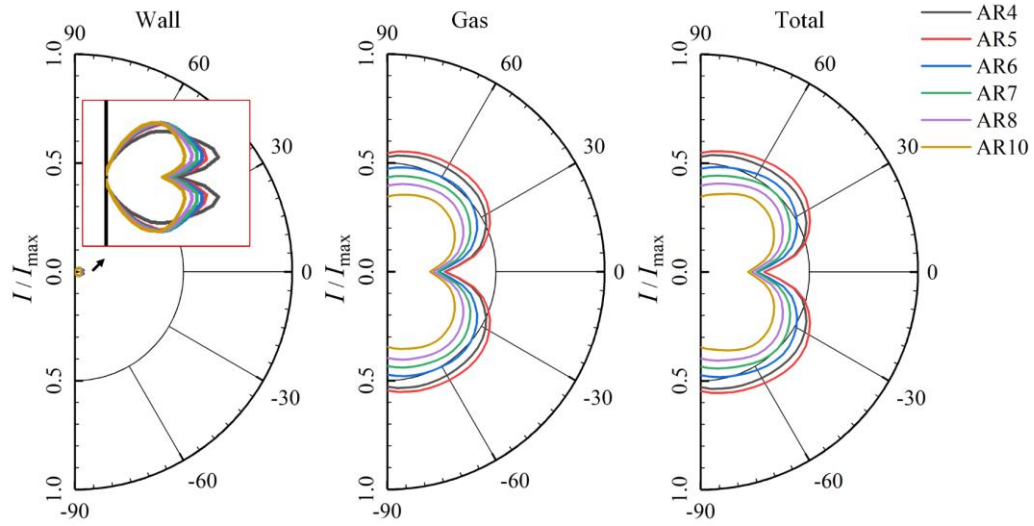
(a)Horizontal Plane (b)Vertical Plane

Figure 16 – Average and peak radiation intensities for multi-stream serpentine nozzles with different SRs

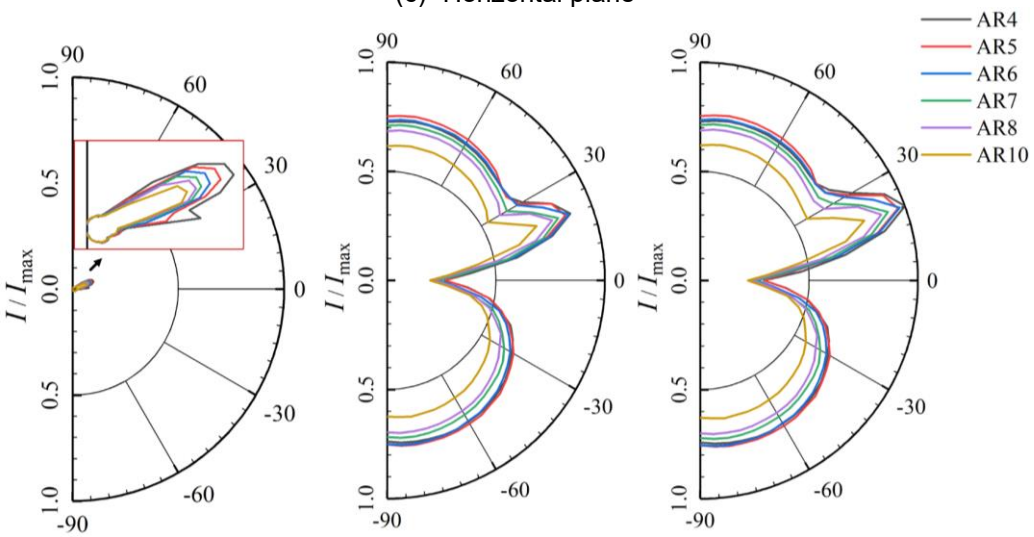
4.3 Aspect Ratio

The aspect ratio (AR) is another key geometric parameter that determines the cross-sectional shape and infrared radiation characteristics of the exhaust system. Based on the baseline multi-stream serpentine nozzle ($AR = 4$), while keeping other design parameters constant, multi-stream serpentine nozzle models with ARs of 5, 6, 7, 8, and 10 were established by solely increasing the cross-sectional width of the mainstream section and decreasing its height. Figure 17 presents the spatial distribution of the infrared radiation intensity of the nozzles with different aspect ratios in the horizontal and vertical detection planes.

As can be observed from the figure, with the increase of the aspect ratio, the gas radiation of the nozzle is effectively suppressed at the vast majority of detection angles. Regarding the wall radiation, its evolution with respect to the aspect ratio exhibits an angular dependence. Within the range of small detection angles, increasing the aspect ratio can effectively weaken the wall radiation; however, in lateral or high-elevation angle regions, the wall radiation inversely exhibits a certain degree of increase. Overall, the holistic infrared signature of the multi-stream serpentine nozzle remains dominated by gas radiation, and the overall infrared signature presents a monotonic downward trend as the aspect ratio increases. Furthermore, the alteration of the geometric aspect ratio does not lead to a significant shift in the spatial distribution characteristics of the radiation intensity, and the detection angle range corresponding to the high-radiation zone remains fundamentally unchanged.



(c) Horizontal plane



(d) Vertical plane

Figure 17 – Spatial distribution of IR radiation intensity for multi-stream serpentine nozzles with different ARs

To elucidate the influence mechanism of the aspect ratio on the infrared radiation characteristics of the multi-stream serpentine nozzle, Fig. 18 compares the plume temperature distribution contours for configurations with different aspect ratios at $\alpha = 90^{\circ}$ in the vertical detection plane. It can be seen from the figure that as the aspect ratio increases from 4 to 10, the shape of the nozzle exit becomes flatter, which significantly increases the wetted perimeter while maintaining a constant exit area. This flattened geometric feature drastically enhances the shear mixing between the jet plume and the external cold air, effectively shortening the high-temperature core region of the plume. As shown in Fig. 18, with the increase of the aspect ratio, the length of the high-temperature core region of the plume is progressively truncated, and the spatial volume of the plume

is compressed, which subsequently leads to the attenuation of the gas radiation from the plume.

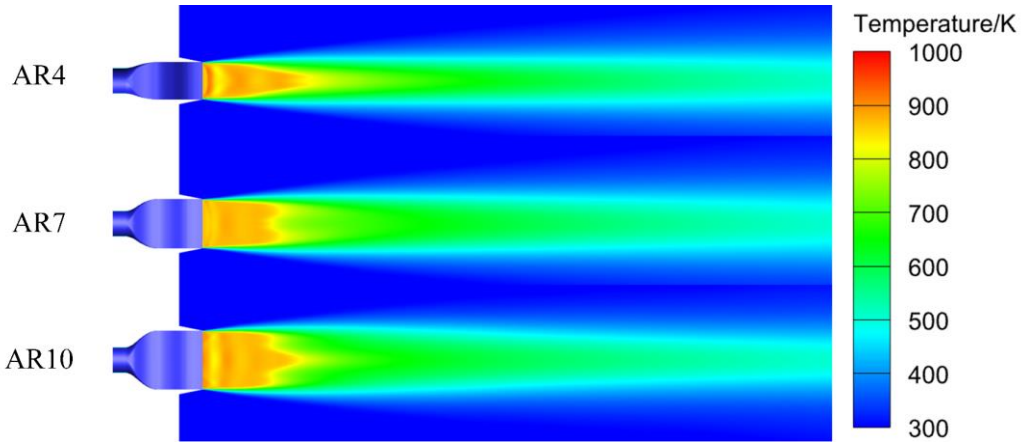
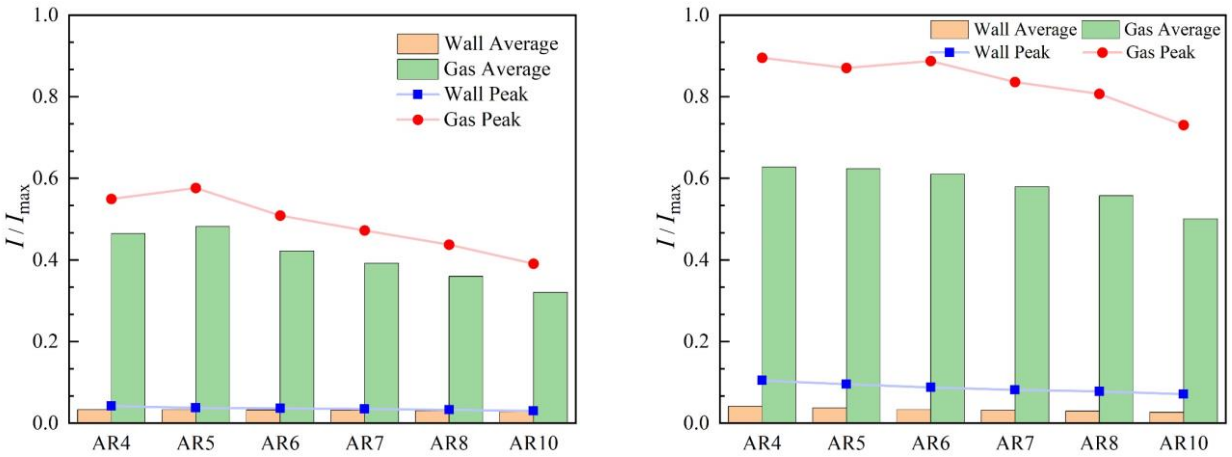


Figure 18 – Plume temperature distribution of configurations with different ARs at 90° in the vertical plane

Figure 19 further provides a quantitative statistical analysis of the evolution laws of the average and peak radiation intensities in different detection planes. Within all the investigated aspect ratio ranges, whether in the horizontal or vertical detection plane, both the average and peak values of gas radiation maintain absolute dominance. As the aspect ratio increases, the average and peak values of gas radiation generally exhibit a clear monotonic downward trend, among which the attenuation in the horizontal detection plane is particularly significant, with a maximum reduction exceeding 30%. Concurrently, although the relevant indicators of wall radiation also exhibit a downward trend with the increase of the aspect ratio (with a reduction reaching approximately 20%), their contribution to the attenuation of the overall infrared signature of the system is not significant due to their relatively low absolute proportion. Furthermore, influenced by the rectangular exit, the overall gas radiation level in the vertical detection plane remains significantly higher than that in the horizontal detection plane under the same aspect ratio configuration.

Based on a comprehensive analysis of the spatial distribution of radiation intensity and temperature distribution characteristics, it can be concluded that although increasing the aspect ratio may introduce a marginal wall radiation increment at certain large lateral viewing angles, it fundamentally weakens the dominant gas radiation by greatly promoting the shear mixing of the exhaust plume. Therefore, in the comprehensive infrared stealth design of multi-stream serpentine nozzles, reasonably adopting a large aspect ratio configuration is an effective approach to suppressing the overall infrared radiation characteristics.



(a)Horizontal Plane (b)Vertical Plane

Figure 19 – Average and peak radiation intensities for multi-stream serpentine nozzles with different ARs

5. Conclusions

Based on numerical simulations, this paper investigates the influence of design parameters on the infrared radiation characteristics of a multi-stream serpentine nozzle. By incorporating the internal occlusion and flow mixing features of the multi-stream serpentine nozzle, the influence laws of the shield ratio and aspect ratio on its IR radiation characteristics are analyzed. The main conclusions are as follows:

1) Under the assumption of uniform inflow without considering the mixer, the high-temperature core gas of the multi-stream serpentine nozzle is fully enveloped by the bypass cold stream. The generation of wall hot-spots is effectively suppressed, resulting in the overall IR signature of the exhaust system being dominated by gas

radiation. Meanwhile, due to the coupling effect of the high-curvature duct in the mainstream section and the flat rectangular exit, the overall gas radiation level in the vertical detection plane is not only significantly higher than that in the horizontal plane but also exhibits strong spatial asymmetric characteristics. This indicates that this configuration possesses superior stealth performance against IR threats from negative detection angles in the vertical detection plane.

2) The SR is a critical factor in truncating the high-temperature visible area and inducing the transition of the dominant mechanism of the exhaust system's IR signature. As the SR increases, the shielding effect of the serpentine configuration on the upstream hot components of the core stream is drastically enhanced, leading to a significant decrease in both the average and peak values of wall radiation, with a maximum reduction exceeding 90%. When the SR reaches 0.55, the internal high-temperature components become completely invisible, thereby substantially weakening the overall radiation intensity of the system. In contrast, because the external exhaust plume is not subjected to the direct physical occlusion of the internal geometry, the attenuation amplitude of its gas radiation is significantly more gradual. This sharp drop in wall radiation, coupled with the relatively gradual variation in gas radiation, drives a fundamental transition in the overall IR signature—shifting the dominant radiation source from the wall to the gas.

3) Increasing the AR is an effective approach to enhance plume mixing and suppress the overall IR signature of the multi-stream serpentine nozzle. At a constant exit area, flattening the nozzle exit increases the wetted perimeter. This actively promotes shear mixing between the high-temperature jet plume and the ambient atmosphere. This effectively truncates the high-temperature core region of the plume and compresses its spatial volume. Driven by this mechanism, both the average and peak values of the dominant gas radiation exhibit a clear monotonic downward trend, with the maximum reduction in the horizontal detection plane exceeding 30%. Furthermore, although a large AR introduces a marginal wall radiation increment during lateral detection, it does not cause any shift in the spatial distribution characteristics of radiation intensity or the dominant radiation source. In summary, in the comprehensive IR stealth design of multi-stream exhaust systems, reasonably adopting a large-AR configuration is an optimal strategy to further suppress the overall IR signature.

6. Contact Author Email Address

mailto: zhouli@mail.nwpu.edu.cn

7. Copyright Statement

The authors confirm that they, and/or their company or organization, hold copyright on all of the original material included in this paper. The authors also confirm that they have obtained permission, from the copyright holder of any third party material included in this paper, to publish it as part of their paper. The authors confirm that they give permission, or have obtained permission from the copyright holder of this paper, for the publication and distribution of this paper as part of the ICAS proceedings or as individual off-prints from the proceedings.

8. Acknowledgements

This study was co-supported by the National Natural Science Foundation of China (No. 52376032) and the National Science and Technology Major Project, China (No. J2019-Ⅱ-0015-0036)

References

[1] ZHENG Junchao, TANG Hailong, CHEN Min, et al. Equilibrium running principle analysis on an adaptive cycle engine[J]. Applied Thermal Engineering, 2018, 132: 393-409.

[2] Sehra A K, Whitlow Jr W. Propulsion and power for 21st century aviation[J]. Progress in aerospace sciences, 2004, 40(4-5): 199-235.

[3] Mahulikar S P, Sonawane H R, Rao G A. Infrared signature studies of aerospace vehicles[J]. Progress in aerospace sciences, 2007, 43(7-8): 218-245.

[4] DENG H W, SHANG S T, JIN H, et al. Analysis and discussion on stealth technology of aero engine[J]. Aeronautical Science & Technology, 2017, 28(10): 1-7 (in Chinese).

[5] Jeong H, Choi B, Kweon I, et al. IR signature characteristics of a turbine engine plume with a 2D nozzle[J]. Infrared Physics & Technology, 2025, 150: 105968.

[6] Shi J, Zhou L, Xu J, et al. Experimental study on infrared radiation characteristics and matching performance of low-observable nozzles[J]. Journal of Propulsion and Power, 2024, 40(3): 354-367.

[7] SHI Jie, ZHOU Li, SHI Jingwei, et al. Infrared radiation signature of three bearing swivel nozzle[J]. Journal of Aerospace Power, 2022, 37(6): 1195-1205. (in Chinese).

[8] Hromisin S M, McLaughlin D K, Morris P J. Effects of nozzle configuration and bypass ratio on the aeroacoustics of dual stream supersonic jets[C]//25th AIAA/CEAS Aeroacoustics Conference, 2019. American Institute of Aeronautics and Astronautics Inc, AIAA, 2019.

[9] Ruscher C J, Magstadt A S, Berry M G, et al. Investigation of a supersonic jet from a three-stream engine nozzle[J]. AIAA journal, 2018, 56(4): 1554-1568.

[10] Younes K, Hickey J P. Indirect noise prediction in compound, multi-stream nozzle flows[J]. Journal of Sound and Vibration, 2019, 442: 609-623.

[11] Meng Y, Shi J, Zhou L, et al. Numerical investigation on flow characteristics of multi-stream supersonic nozzle with serpentine configuration[J]. Aerospace Science and Technology, 2024, 144: 108799.

[12] XU Jianyu, ZHOU Li, SHI Jie, et al. Investigation on infrared radiation characteristics of multi-stream serpentine nozzle[J]. Journal of Aerospace Power, 2025, 40(2): 20230148 doi: 10.13224/j.cnki.jasp. 20230148(in Chinese).

[13] Lee C, Boedicker C. Subsonic diffuser design and performance for advanced fighter aircraft[C]//Aircraft design systems and operations meeting. 1985: 3073.

[14] RIVIÈRE P, SOUFIANI A. Updated band model parameters for H2O, CO2, CH4 and CO radiation at high temperature[J]. International Journal of Heat and Mass Transfer, 2012, 55(13):3349–3358.

[15] TASHKUN S A , PEREVALOV V I .CDSD-4000: Highresolution, high-temperature carbon dioxide spectroscopic databank[J].Journal of Quantitative Spectroscopy and Radiative Transfer, 2011, 112(9): 1403-1410.

[16] ROTHMAN L S, GORDON I E, BARBER R J, et al. HITEMP, the high-temperature molecular spectroscopic database [J]. Journal of Quantitative Spectroscopy & Radiative Transfer, 2010, 111(15): 2139-2150.

[17] Jie SHI, Li ZHOU, Jingwei SHI, Zhanxue WANG. Influence of design parameters on infrared radiation characteristics of serpentine nozzles under complex flow conditions[J]. Acta Aeronautica et Astronautica Sinica, 2024, 45(17): 530082.